PAPER

Uniformly dispersed platinum nanoparticles over nitrogen-doped reduced graphene oxide as an efficient electrocatalyst for the oxygen reduction reaction†

Xiaohong Chen, [a] Zhiyong Xue, *[a] Yafei Zheng, [a] Xundao Liu*[c] and Yongming Zhang*[b]

Oxygen reduction reaction (ORR) with efficient activity and stability is significant for fuel cells. Herein, platinum (Pt) nanoparticles dispersed on nitrogen-doped reduced graphene oxide (N-rGO) were prepared by a hydrothermal and carbonized approach for the electrocatalysis of ORR. Polyvinylpyrrolidone plays a significant role in the reduction and dispersion of platinum particles (about 2 nm). The obtained Pt–N-rGO hybrids exhibited superior activity with an electron transfer number of ~4.0, onset potential 0.90 eV of ORR, good stability and methanol tolerance in alkaline media. These results reveal the interactions between Pt–N-rGO and oxygen molecules, which may represent an oxygen modified growth in catalyst preparation. The excellent electrocatalysis may lead to the decreased consumption of expensive Pt and open up new opportunities for applications in lithium air batteries.

1 Introduction

Oxygen reduction reaction (ORR) catalysts are significant barriers to the widespread use of fuel cells.[1–8] Platinum (Pt)-based materials are the state-of-the-art ORR catalysts, which endow better catalyst performance with CO poisoning, high cost, agglomeration, Pt dissolution, and less availability.[9–11] Hence, great efforts have been made to resolve these issues of ORR catalysts, which can enhance the activity and stability of Pt hampered by its agglomeration and diameter size.[12–18] Some researchers have designed to replace Pt nanoparticles with uniform distribution on porous carbon materials, which are inexpensive, easily obtained, good biocompatibility and large specific surface area.[19–21]

Pt nanoparticles (Pt NPs) were prepared by various methods to obtain uniform size of Pt NPs and enhance the ORR activity. Huang[22] reported Pt nanocrystals synthesized in an aqueous solution at 85 °C by a fresh NaBH$_4$ solution. When carbon black particles were inserted into the reduced graphene oxide (rGO) sheets, the stacking of rGO can be effectively prevented, which

can promote diffusion of oxygen molecules through the rGO sheets to improve the ORR electrocatalytic activity. Li[23] reported a mild and environmental friendly reductant, ethylene glycol, which was used as both a reductive and dispersing agent for the deposition of Pt nanoparticles on GO sheets, which show higher electrocatalytic activity. Yamauchi[24] reported mesoporous Pt nanorods synthesized by a electrochemical method, which also exhibited high activity and CO-tolerant performance in the electro-oxidation of methanol. Chen[25] reported that Pt NPs can be stabilized by trifluoromethylphenyl groups (Pt–Ar–CF$_3$), which show the highest catalytic activity and high ORR specific activity. This enhanced activity is attributed to the weakened oxygen adsorption by the electronegative ligands. Although various preparation methods from Pt nanoparticles were reported, the polyvinylpyrrolidone (PVP) reduction of platinum particles has rarely been reported.

A series of heteroatom-doped carbon materials as the support of Pt NPs is applied to enhance catalytic activity.[26–31] Wang[32] reported nanocarbon-wedged N-doped graphene (NWGN) can provide numerous between-plane electrolyte diffusion channels to favor the transport of water and reaction species. The doped N atoms in the carbon sheets can further provide more binding sites for Pt NPs on NWGN surfaces. With loading on graphene, the troubles of dissolution, sintering, and agglomeration of Pt NPs during electrochemical processes can be efficiently avoided. However, the high surface area and efficient heteroatoms doping for Pt-heteroatom-doped carbon materials are urgently needed in the fuel cell field.

[a]*Institute for Advanced Materials, North China Electric Power University, Beijing, China. E-mail: xuezy@ncepu.edu.cn*

[b]*School of Chemistry and Chemical Engineering, Shanghai Jiao Tong University, No. 800 Dongchuan Rd., Minhang District, Shanghai 200240, China. E-mail: ymzsjtu@gmail.com*

[c]*School of Materials Science and Engineering, University of Jinan, Jinan, 250022, China. E-mail: mse_liuxundao@ujn.edu.cn*

† Electronic supplementary information (ESI) available. See DOI: 10.1039/d1ra04857k

Herein, the Pt NPs of uniform size dispersed on N-doped reduced graphene (Pt–N-rGO) were successfully obtained by a hydrothermal and carbonized approach. More importantly, PVP plays a significant role in preparation and evenly dispersing on the reduced graphene of Pt NPs (about 2.0 nm), which attributes to the dispersibility and reduction from PVP. Therefore, the Pt–N-rGO hybrids are used as ORR electrocatalysts and exhibit excellent activity with an electron transfer number of ~4, onset potential (0.90 eV), good stability and methanol tolerance in a KOH solution. The high ORR performance, convenient preparation, large surface area and high N content of Pt–N-rGO indicate the promising potential in fuel cell and lithium air battery fields.

2   Experimental

Materials

Polyvinylpyrrolidone (PVP, $M_w = 300\,000$) was acquired from J&K scientific Chemical Co., Ltd. Chloroplatinic acid hexahydrate ($H_2PtCl_6 \cdot 6H_2O$) was bought from Shanghai Titanchem Co., Ltd. Potassium hydroxide (KOH), dicyandiamide, ethanol and methanol were purchased from Sinopharm Chemical Reagent CO., Ltd. A 5 wt% Nafion® solution was purchased from E. I. DuPont Company. All solutions used in the electrochemical experiments were freshly prepared with Millipore water (resistivity = ~18.2 MΩ).

Apparatus

Transmission electron microscope (TEM, JEM-2010HT), scanning electron microscopy (SEM, JEOL2100F) (both from Electron Optics Laboratory Co., Ltd., Japan), powder X-ray diffractometer (XRD, Bruker, German, APLX-DUO), Raman spectrometer (Thermo Fisher H31XYZE-US), X-ray photoelectron spectroscopy (XPS, AXIS UltraDLD), Brunauer–Emmett–Teller (BET, ASAP 2460), electrochemical workstation (Autolab PGSTAT302N, Metrohm, Switzerland and CHI 660D, Chenhua, China), inductively coupled plasma emission spectrometer (ICP, Avio 500, PerkinElmer, Singapore).

Synthesis of reduced graphene oxide (rGO)

We used high-purity nitrogen as protective ambient to anneal a mixture of GO. The detailed procedure is as follows: GO powders were placed at the center of a quartz tube under nitrogen flow. Before the furnace was heated to 900 °C, N_2 gas was flowed for about 20 min. When the center of the furnace reached the designed reaction temperature for 1 h, the sample was cooled to room temperature under N_2 ambient to obtain products (65.0%).

Synthesis of Pt-rGO and Pt–N-rGO hybrids

0.1 g GO, H_2PtCl_6 (5.30 mL, 1 g/100 mL), 0.1 g PVP and 40 mL deionized water were successively added into a 100 mL Teflon stainless steel autoclave, which was treated by a hydrothermal way at 110 °C for 24 h. Then, the mixture was obtained after drying at 80 °C in an oven. Stabilization and carbonization of the above mixture were placed in the center of a quartz tube

under N_2 flow. After carrying out N_2 flow for 20 min, the dried mixture was heated to 900 °C and annealed for 2 h, and then cooled to room temperature to obtain Pt-rGO hybrids (63.0%).

In addition, dicyandiamide (45.00 mg) was added in the hydrothermal treatment. Pt–N-rGO hybrids (60.0%) were obtained according to the above Pt-rGO hybrid procedure. For comparison, the Pt-rGO-2 (64.0%) and Pt–N-rGO-2 (62.0%) hybrids were prepared according to the above Pt-rGO hybrids procedure, without PVP.

Preparation of rGO, Pt-rGO and Pt–N-rGO hybrids modified electrode

Before use, the glassy carbon electrode (GCE, $\varphi = 3$ mm) was polished with Al_2O_3 powders and washed thoroughly with deionized water to remove Al_2O_3 residues, and then dried at room temperature. 4 μL of 1 mg mL^{-1} sonicated rGO, Pt-rGO and Pt–N-rGO hybrids with ethanol and water suspension (8 : 2) and Nafion solution (10 μL, 5.0 wt%) was dropped on the pretreated bare GCE or GC disk using a micropipet tip and dried in air.

Cyclic voltammograms (CV) measurement

CV measurement was conducted at 25 °C using an Autolab PGSTAT302 (Metrohm) electrochemical test system using saturated RHE as the reference electrode, a Pt wire as the counter electrode and the sample modified glassy carbon electrode as the working electrode. A 0.1 M KOH aqueous solution was used as the electrolyte, which was saturated with O_2 by bubbling it prior to the start of each experiment. A flow of O_2 was maintained over the electrolyte during the recording of CVs in order to ensure continuous O_2 saturation. The working electrode was cycled at least 5 times before data recorded at a scan rate of 10 mV s^{-1}. CV measurements were also performed under N_2 atmosphere in control experiments.

Rotating disk electrode (RDE) measurement

For the RDE measurement, catalyst inks were prepared by the same method as that of CV analysis described above. 4 μL of 5 mg mL^{-1} ink was loaded on a glassy carbon RDE ($\varphi = 3$ mm). The working electrode was cathodically scanned at a rate of 10 mV s^{-1} with varying rotating speeds from 400 to 2000 rpm. The ORR current was determined by subtracting the N_2 current from the O_2 current. Koutecky–Levich (K–L) plots were analyzed at various electrode potentials. The slopes of their best linear fit lines were used to calculate the electron transfer number (n) on the basis of the K–L equation:

$$B = 0.62nFC_0(D_0)^{2/3}v^{-1/6} \quad J_K = nFkC_0$$

where J is the measured current density, J_K and J_L are the kinetic and diffusion limiting current densities, respectively, ω is the angular velocity, n is the transferred electron number, F is the Faraday constant (96 485 C mol^{-1}), C_0 is the bulk concentration of O_2 (1.2×10^{-3} mol cm^{-3}), D_0 is the diffusion coefficient of O_2 (1.9×10^{-5}), v is the kinematic viscosity of the electrolyte (0.01 m^2 s^{-1}), and k is the electron-transfer rate constant.

3   Results and discussion

The Pt NPs loaded on N-doped reduced graphene (Pt–N-rGO) were synthesized by a hydrothermal treatment and then carbonization at 900 °C under nitrogen atmosphere,[33] yielding the final sample Pt–N-rGO hybrids. As shown in Fig. 1, rGO and Pt-rGO hybrids showed a wrinkled surface, and then the Pt–N-rGO hybrids clearly showed that Pt NPs evenly dispersed on the N-rGO micro-morphology *via* scanning electron microscopy (SEM). The diameter of the Pt NPs is about 2 nm, which is beneficial to improve the electrocatalytic activity. Furthermore, the energy dispersive spectroscopy (EDS) spectrum (Fig. 1E) of Pt–N-rGO hybrids also indicates the presence of N (10.8 wt%) and Pt elements. Furthermore, the precise determination of the Pt content of Pt-rGO and Pt–N-rGO hybrids was 15.4 wt% and 14.1 wt%, respectively, obtained from the ICP experiments, which confirmed that the nitrogen doping graphene did not influence the Pt deposition, indicated its better charge conductivity and offered active sites for ORR. These results further confirm the Pt decorated on the N doping of rGO.

The porosity and pore volume from those hybrids are of great importance for the enhanced ORR performance. BET measurements of rGO, Pt-rGO and Pt–N-rGO hybrids were performed to obtain the N_2 isotherms and their pore size distribution curves. As shown in Fig. S1–S3,† the surface area of Pt–N-rGO hybrids is 287.16 m^2 g^{-1}, which is higher than that of rGO (75.84 m^2 g^{-1}) and Pt-rGO (242.63 m^2 g^{-1}). Moreover, the pore size of Pt–N-rGO is smaller, compared with that of rGO and Pt-rGO hybrids. Those results indicated that there are numerous active sites to improve the ORR performance.

From the high-resolution transmission electron microscopy (HRTEM) images of Pt–N-rGO hybrids (Fig. 2), the diameter sizes and shape distribution of Pt NPs were about 2 nm, which were evenly loaded on N-rGO. Moreover, Fig. 2C shows the lattice fringes with a d-spacing of 2.28 Å, indicating the crystal growth of face-centered cubic (fcc) Pt {111} planes loaded on N-rGO.[34] The Pt-rGO and Pt–N-rGO hybrids were obtained without PVP. From the TEM images of Pt-rGO-2 and Pt–N-rGO-2 (Fig. S4†), uneven size and dispersion of Pt nanoparticles were loaded on rGO. In particular, the size of Pt nanoparticles is from 5.5 to 28.0 nm. Therefore, PVP plays an important role in the
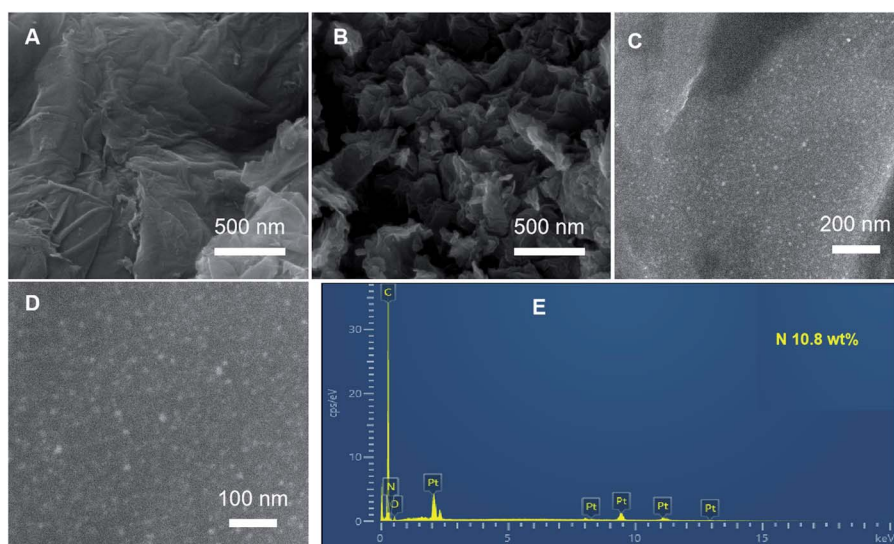

Fig. 1   SEM images of (A) rGO, (B) Pt-rGO and (C, D) Pt–N-rGO hybrids. (E) EDS spectrum of Pt–N-rGO hybrids.
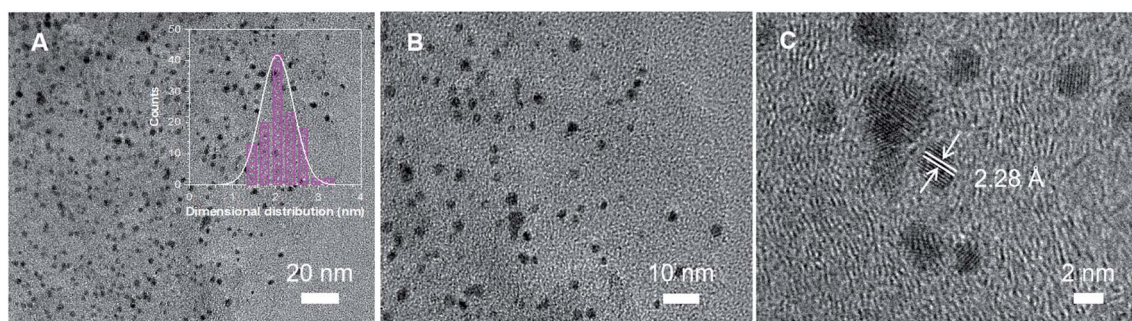

Fig. 2   (A–C) TEM images of Pt–N-rGO hybrids at different magnifications; inset image is the particle size distribution of Pt NPs in Pt–N-rGO hybrids.
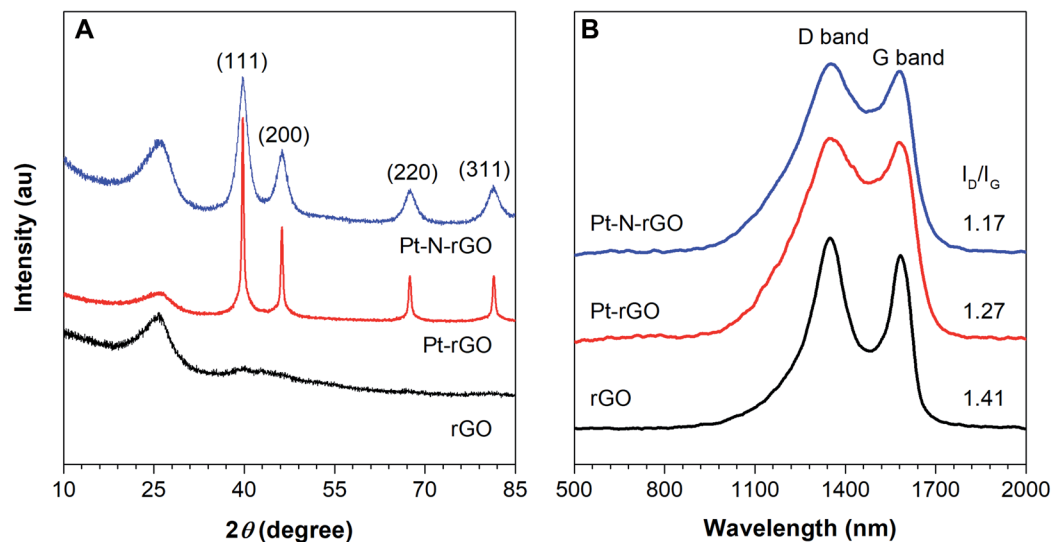
Fig. 3 The (A) XRD and (B) Raman spectra of rGO, Pt-rGO and Pt–N-rGO hybrids.

uniform size and dispersion of Pt nanoparticles on rGO. These results sharply contribute to improve the catalytic activity of ORR performance.

The preparation of Pt–N-rGO hybrids was successfully validated by X-ray diffraction (XRD) patterns. It can be seen from Fig. 3A that the peak located at 25.7° is evident for rGO, N-rGO, and Pt–N-rGO hybrids, which are attributed to the graphite

crystalline plane. Moreover, all Pt peaks located at 40.2, 46.3, 67.8 and 81.2° appeared from Pt-rGO and Pt–N-rGO (JPDS#PDF#65-2868), which are consistent with the typical face-centered-cubic (111), (200), (220) and (311) crystalline planes of Pt NPs,[35] respectively, and identified from the diffraction pattern of the resulting rGO. The Raman spectra of rGO, Pt-rGO, and Pt–N-rGO hybrids are also observed in Fig. 3B.
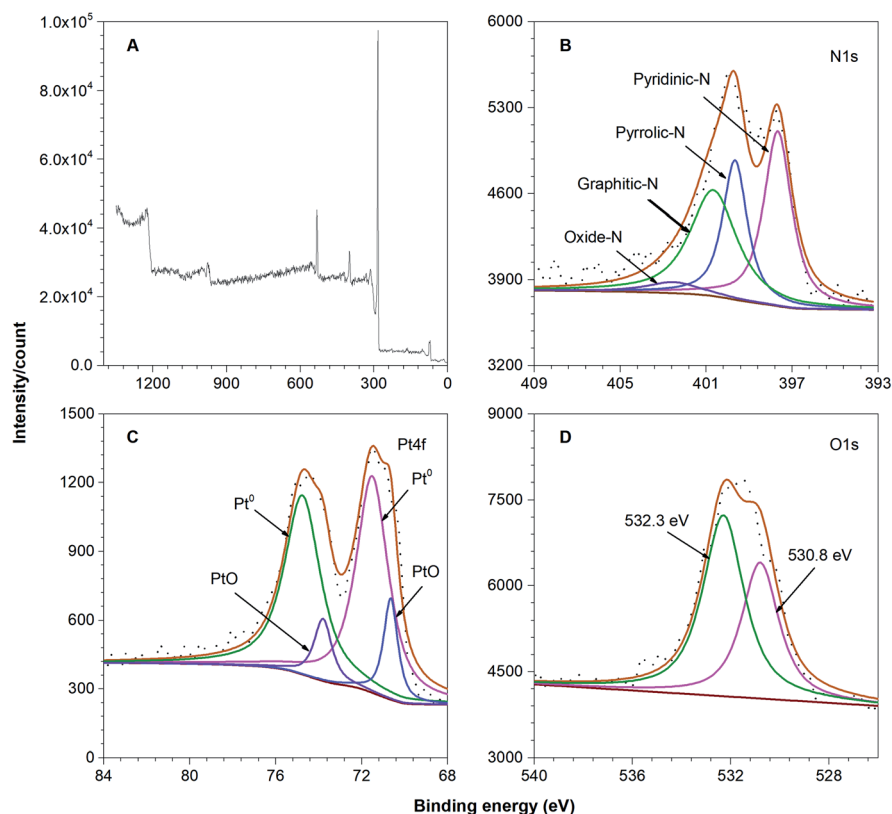

Fig. 4 XPS spectra of the (A) survey scan, (B) N 1s region, (C) Pt 4f region and (D) O 1s region of the Pt–N-rGO hybrids.

All the samples displayed three Raman peaks located at 1357 and 1580 cm^{-1}, which correspond to the disordered (D band) and graphitic (G band) of carbon. The I_D/I_G band intensity ratio of Pt–N-rGO is 1.17, which is lower than that of rGO (1.41) and Pt-rGO (1.27), and indicated the sharp graphitization, suggesting that a large amount of N and Pt atoms could be doped in rGO.[36] Such an improved graphitic structure would offer enhanced conductivity of Pt–N-rGO, which is conductive to the ORR performance.

To validate N and Pt codoping in rGO, the XPS survey spectrum of Pt–N-rGO hybrids clearly exhibited the presence of N 1s and Pt 4f peaks (Fig. 4). As shown in Fig. 4B, the typical N 1s spectrum can be deconvoluted into four types: pyridinic-N 397.7 eV (35.2%), pyrrolic-N 399.7 eV (24.4%), graphitic nitrogen-N 400.7 eV (35.8%), and oxidized nitrogen-N 402.7 eV (4.3%), respectively, indicating that pyridinic-N and graphitic nitrogen-N are predominant in Pt–N-rGO hybrids and contribute to the adsorption of oxygen molecules and provide much more active sites due to the higher positive charge and spin density of carbon atoms to offer better ORR performance.

Moreover, in the spectrum of Pt 4f (Fig. 4C), there are two peaks, which can be deconvoluted into two types. The peak binding energies of Pt $4f_{7/2}$ and $4f_{5/2}$ of Pt (0) at 70.3 eV and 73.8 eV, respectively, result from Pt NPs. Two weaker doublets at 71.5 eV and 74.8 eV of Pt(II) species (such as PtO) are also present,[37] which can be attributed to the slight oxidation of Pt NPs upon exposure to air. These results suggest that metallic Pt (0) is the predominant species in the Pt–N-rGO hybrids. In addition, the peak at 530.8 eV probably corresponds to the oxygen species (PtO), and that at 532.3 eV is assignable to the residual oxygen containing groups (such as OH and COOH) on the surface of Pt–N-rGO hybrids (Fig. 4D). The XPS results of Pt–N-rGO hybrids further confirm the successful preparation of Pt–N-rGO hybrids.

To get more catalytic activity information of rGO, Pt-rGO and Pt–N-rGO catalysts in ORR, cyclic voltammograms (CVs) and electrochemical measurements on a RDE were performed. As shown in Fig. 5A, rGO, Pt-rGO and Pt–N-rGO exhibited electrocatalytic ORR activity. There is a more positive ORR of Pt–N-rGO hybrids with an onset potential at 0.72 V than that of rGO (0.68 V) and Pt-rGO (0.67), indicating synergistic ORR catalytic activity of nitrogen and Pt NPs in the Pt–N-rGO hybrids.[38,39]

To further reveal the reaction kinetics for rGO, Pt-rGO and Pt–N-rGO hybrids, linear sweep voltammograms (LSVs) were performed at a scan rate of 10 mV s^{-1} in an O$_2$-saturated 0.1 M KOH electrolyte using a rotating disk electrode (RDE) (Fig. 5B
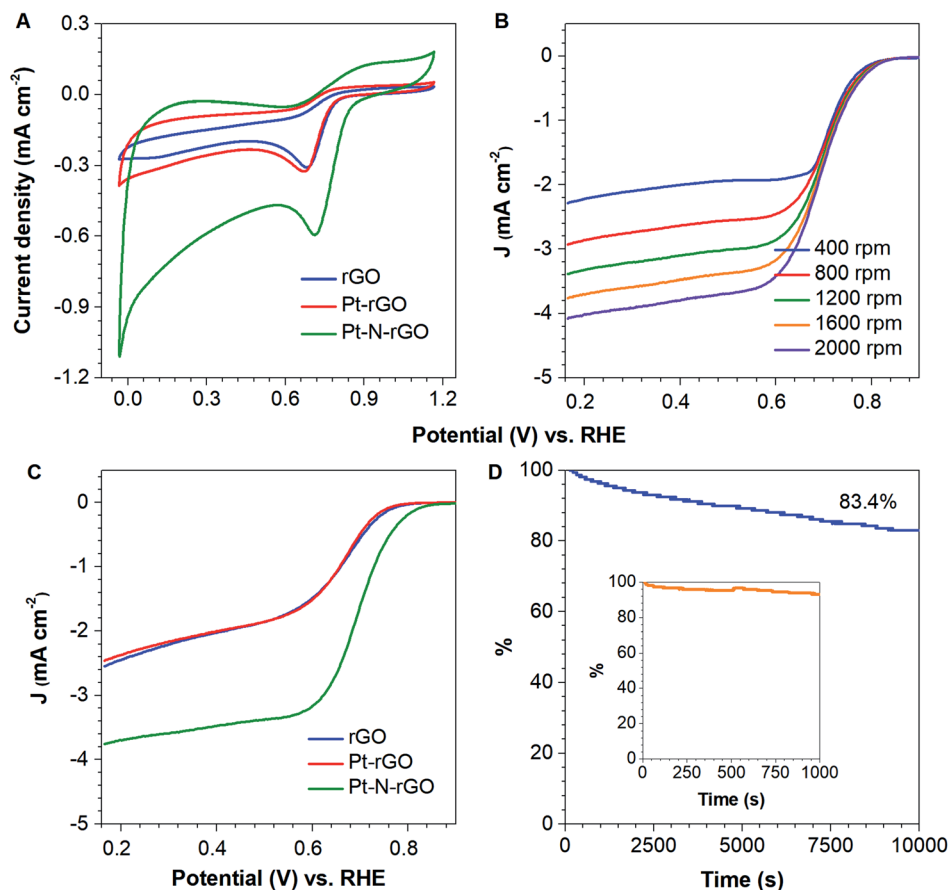

Fig. 5 (A) Cyclic voltammograms of rGO, Pt-rGO and Pt–N-rGO hybrids recorded in an O$_2$-saturated 1 M KOH solution at a scan rate of 10 mV s^{-1}. LSVs of (B) Pt–N-rGO hybrids at different rotation speeds and (C) rGO, Pt-rGO and Pt–N-rGO hybrids in the O$_2$-saturated 0.1 M KOH solution at a scan rate of 10 mV s^{-1}. (D) Chronoamperometric response of Pt–N-rGO hybrids is kept at 0.62 V in the O$_2$-saturated 0.1 M KOH solution, inset spectrum: chronoamperometric response of Pt–N-rGO hybrids is kept at 0.62 V with 3 wt% methanol addition at 200 s. The rotation speed is at 1600 rpm.

and C). The rGO, Pt-rGO and Pt–N-rGO hybrids showed an increasing ORR performance with onset potentials at 0.83 V, 0.83 V and 0.90 V, respectively. The half-wave potentials were 0.62 V, 0.63 V and 0.64 V, respectively, due to the synergistic effects of N doping, rGO and Pt NPs, more activity sites and effective electrical conductivity.[40]

Moreover, RDE curves of rGO, Pt-rGO and Pt–N-rGO at various rotation speeds were performed to validate its ORR kinetic performance in 0.1 M KOH (Fig. 5B, S5 and S7†). The linearity and parallelism of the Koutecky–Levich plots suggested reaction kinetics towards the concentration of dissolved oxygen and electron transfer numbers (n) for ORR at different potentials (Fig. S6, S8 and S9†). The n of rGO, Pt-rGO and Pt–N-rGO were calculated to be 2.76, 2.60 and 3.90, respectively, at 0.2 V from the slopes of K–L plots, indicating those materials can favour the ~4e oxygen reduction process.

Furthermore, the long-term stability of catalysts plays an important role in fuel cell technology. The durability of Pt–N-rGO catalysts was tested at a constant voltage of 0.62 V for 10 000 s in O_2-saturated 0.1 M KOH (Fig. 5D). The chronoamperometric response of Pt–N-rGO under alkaline conditions also retained a higher relative current of ~83.4%. The better durability of Pt–N-rGO hybrids is ascribed to the unique Pt NPs within rGO, which not also enhance their interfacial contact, but suppress the agglomeration of Pt NPs, to facilitate the transport of electrolyte ions. In addition, when the methanol solution was injected into the 0.1 M KOH solution at 200 s, the chronoamperometric curves y of Pt–N-rGO hybrids showed no change (Fig. 5D inset spectrum), indicated that Pt–N-rGO hybrids possess better tolerance, due to the accumulation of methanol oxidation reaction intermediates did not happen on the Pt–N-rGO surface.

4 Conclusions

In summary, Pt–N-rGO hybrids were easily synthesized by hydrothermal treatment and carbonization method, for oxygen reduction reaction materials. Pt NPs evenly dispersed on N-rGO. Interestingly, Pt NPs were successfully reduced and dispersed by PVP. The N-rGO endows Pt NPs with uniform distribution and much more specific surface area. These results indicated Pt–N-rGO exhibited great electrocatalytic activity and better durability for ORR in alkaline electrolytes. This is attributed to the synergistic effects of N doping, rGO and Pt NPs. This synthetic strategy of Pt–N-rGO hybrids may be further extended to prepare other metal or metal oxides/carbon-based materials for various applications, such as fuel cell, lithium-air battery, and supercapacitor fields.

Conflicts of interest

There are no conflicts to declare.

Acknowledgements

References

1 J. M. Kim, J. H. Kim, J. Kim, Y. Lim, Y. Kim, A. Alam, J. Lee, H. Ju, H. C. Ham and J. Y. Kim, *Adv. Mater.*, 2020, **32**, 2002210.

2 Z. Zhu, H. Yin, Y. Wang, C. Chuang, L. Xing, M. Dong, Y. Lu, G. C. Garcia, Y. Zheng, S. Chen, Y. Dou, P. Liu, Q. Cheng and H. Zhao, *Adv. Mater.*, 2020, **32**, 2004670.

3 H. Meng, Y. Liu, H. Pei, S. Yuan, X. Li, H. Zhang and Y. Zhang, *ACS Appl. Mater. Interfaces*, 2020, **12**, 41580.

4 X. Liu, D. Wu, X. Liu, X. Luo, Y. Liu, Q. Zhao, J. Li and D. Dong, *Electrochim. Acta*, 2020, **336**, 135757.

5 G. Zhang, Y. Xu, X. Xiang, G. Zheng, Z. Li, T. Rena and Y. Zhang, *Tribol. Int.*, 2018, **126**, 39.

6 X. Liu, X. Luo, X. Chen, S. Zou, X. Liu, J. Li, H. Li and D. Dong, *J. Electroanal. Chem.*, 2020, **871**, 114283.

7 H. Meng, X. Chen, T. Gong, H. Liu, Y. Liu, H. Li and Y. Zhang, *Chem. Phys.*, 2019, **11**, 6015.

8 X. Chen, L. Huang, J. Liu, D. Song and S. Yang, *Energy*, 2022, **239**, 121897.

9 Z. Y. Zhou, X. Kang, Y. Song and S. Chen, *J. Phys. Chem. C*, 2012, **116**, 10592.

10 J. Choi, H. S. Kim, Y. J. Sohn, S. D. Yim, F. M. Alamgir and S. S. Jang, *ACS Appl. Nano Mater.*, 2021, **4**, 1067.

11 Y. Xiong, M. You, F. Liu, M. Wu, C. Cai, L. Ding, C. Zhou, M. Hu, W. Deng and S. Wang, *ACS Appl. Energy Mater.*, 2020, **3**, 2490.

12 L. Zhao, X. L. Sui, J. L. Li, J. J. Zhang, L. M. Zhang and Z. B. Wang, *ACS Appl. Mater. Interfaces*, 2016, **8**, 16026.

13 J. Hu, R. Li, S. Zhu, G. Zhang and P. Zhu, *Cellulose*, 2021, **28**, 4991.

14 X. Ren, Y. Wang, A. Liu, Z. Zhang, Q. Lv and B. Liu, *J. Mater. Chem. A*, 2020, **8**, 24284.

15 Q. Wang, L. Zhang, Y. Liu, G. Zhang and P. Zhu, *Carbohydr. Polym.*, 2020, **232**, 115693.

16 Q. Huang, Y. Guo, D. Chen, L. Zhang, T.-T. Li, Y. Hu, J. Qian and S. Huang, *Chem. Eng. J.*, 2021, **424**, 130336.

17 X. Wang, L. Chai, J. Ding, L. Zhong, Y. Du, T.-T. Li, Y. Hu, J. Qian and S. Huang, *Nano Energy*, 2019, **62**, 745.

18 X. Wang, A. Dong, Z. Zhu, L. Chai, J. Ding, L. Zhong, T.-T. Li, Y. Hu, J. Qian and S. Huang, *Small*, 2020, **16**, 2004614.

19 X. Chen, Z. Xue, K. Niu, X. Liu, W. Lv, B. Zhang, Z. Li, H. Zeng, Y. Ren, Y. Wu and Y. Zhang, *RSC Adv.*, 2021, **11**, 4053.

20 G. Zhang, Y. Xu, X. Xiang, G. Zheng, X. Zeng, Z. Li, T. Ren and Y. Zhang, *Tribol. Int.*, 2018, **126**, 39.

21 H. Fei, J. Dong, D. Chen, T. Hu, X. Duan, I. Shakir, Y. Huang and X. Duan, *Chem. Soc. Rev.*, 2019, **48**, 5207.

22 Y. Li, Y. Li, E. Zhu, T. McLouth, C. Y. Chiu, X. Huang and Y. Huang, *J. Am. Chem. Soc.*, 2012, **134**, 12326.

23 Y. Li, W. Gao, L. Ci, C. Wang and P. M. Ajayan, *Carbon*, 2010, **48**, 1124.

24 C. Li, T. Sato and Y. Yamauchi, *Angew. Chem., Int. Ed.*, 2013, **52**, 8050.

25 Z. Zhou, X. Kang, Y. Song and S. Chen, *J. Phys. Chem. C*, 2012, **116**, 10592.

26 K. K. Karuppanan, A. V. Raghu, M. K. Panthalingal, V. Thiruvenkatam, K. Pc and B. Pullithadathil, *Sustainable Energy Fuels*, 2019, **3**, 996.

27 J. Ma, A. Habrioux, Y. Luo, G. R. Sanchez, L. Calvillo, G. Granozzi, P. B. Balbuena and N. A. Vante, *J. Mater. Chem. A*, 2015, **3**, 11891.

28 A. Mahata, A. S. Nair and B. PathakCatal, *Sci. Technol.*, 2019, **9**, 4835.

29 J. Park, Y. J. Jang, Y. J. Kim, M. Song, S. Yoon, D. H. Kim and S. J. Kim, *Phys. Chem. Chem. Phys.*, 2014, **16**, 103–109.

30 P. Q. Phan, R. Naraprawatphong, P. Pornaroontham and J. Park, *Adv. Mater.*, 2021, **2**, 322.

31 S. Sui, X. Wang, X. Zhou, Y. Suc, S. Riffatc and C. Liu, *J. Mater. Chem. A*, 2017, **5**, 1808.

32 Y. Xiong, M. You, F. Liu, M. Wu, C. Cai, L. Ding, C. Zhou, M. Hu, W. Deng and S. Wang, *ACS Appl. Energy Mater.*, 2020, **3**, 2490.

33 X. Chen, Z. Ning, Z. Zhou, X. Liu, J. Lei, S. Pei and Y. Zhang, *RSC Adv.*, 2018, **8**, 27246.

34 L. Cao, G. Zhang, S. Jiang, X. Tang, X. Qin, X. Guo, Z. Shao and B. Yi, *ChemElectroChem*, 2016, **3**, 309.

35 D. A. Robinson and K. J. Stevenso, *J. Mater. Chem. A*, 2013, **1**, 13443.

36 J. Yan, Y. Wang, Y. Zhang, S. Xia, J. Yu and B. Ding, *Adv. Mater.*, 2020, **33**, 2007525.

37 L. Du, S. Zhang, G. Chen, G. Yin, C. Du, Q. Tan, Y. Sun, Y. Qu and Y. Gao, *ACS Appl. Mater. Interfaces*, 2014, **6**, 14043.

38 A. Arunchander, S. G. Peera, V. Parthiban, S. Akula, T. Kottakkat, S. D. Bhat and A. K. Sahu, *RSC Adv.*, 2015, **5**, 75218.

39 Z. Duan and G. Wang, *J. Phys. Chem. C*, 2013, **117**, 6284.

40 J. Choi, Y. J. Lee, D. Park, H. Jeong, S. Shin, H. Yun, J. Lim, J. Han, E. J. Kim, S. S. Jeon, Y. Jung, H. Lee and B. J. Kim, *Energy Environ. Sci.*, 2020, **13**, 4921.